Spontaneous fission modes and lifetimes of superheavy elements in the nuclear density functional theory

A. Staszczak,[1,2,3] A. Baran,[1,2,3] and W. Nazarewicz[2,3,4]

[1]*Institute of Physics, Maria Curie-Skłodowska University, pl. M. Curie-Skłodowskiej 1, 20-031 Lublin, Poland*

[2]*Department of Physics and Astronomy, University of Tennessee Knoxville, Tennessee 37996, USA*

[3]*Oak Ridge National Laboratory, P.O. Box 2008, Oak Ridge, Tennessee 37831, USA*

[4]*Theoretical Physics, University of Warsaw, ul. Hoża 69, 00-681 Warsaw, Poland*

(Received 26 July 2012; revised manuscript received 1 February 2013; published 27 February 2013)

Background: The reactions with the neutron-rich ^{48}Ca beam and actinide targets resulted in the detection of new superheavy (SH) nuclides with $Z = 104$–118. The unambiguous identification of the new isotopes, however, still poses a problem because their α-decay chains terminate by spontaneous fission (SF) before reaching the known region of the nuclear chart. The understanding of the competition between α-decay and SF channels in SH nuclei is, therefore, of crucial importance for our ability to map the SH region and to assess its extent.

Purpose: We perform self-consistent calculations of the competing decay modes of even-even SH isotopes with $108 \leqslant Z \leqslant 126$ and $148 \leqslant N \leqslant 188$.

Methods: We use the state-of-the-art computational framework based on self-consistent symmetry-unrestricted nuclear density functional theory capable of describing the competition between nuclear attraction and electrostatic repulsion. We apply the SkM* Skyrme energy density functional. The collective mass tensor of the fissioning superfluid nucleus is computed by means of the cranking approximation to the adiabatic time-dependent Hartree-Fock-Bogoliubov (HFB) approach. This paper constitutes a systematic self-consistent study of spontaneous fission in the SH region, carried out at a full HFB level, that simultaneously takes into account both triaxiality and reflection asymmetry.

Results: Breaking axial symmetry and parity turns out to be crucial for a realistic estimate of collective action; it results in lowering SF lifetimes by more than 7 orders of magnitude in some cases. We predict two competing SF modes: reflection symmetric modes and reflection asymmetric modes.

Conclusions: The shortest-lived SH isotopes decay by SF; they are expected to lie in a narrow corridor formed by ^{280}Hs, ^{284}Fl, and $^{284}_{118}$Uuo that separates the regions of SH nuclei synthesized in "cold-fusion" and "hot-fusion" reactions. The region of long-lived SH nuclei is expected to be centered on ^{294}Ds with a total half-life of $\sim$1.5 days. Our survey provides a solid benchmark for the future improvements of self-consistent SF calculations in the region of SH nuclei.

DOI: 10.1103/PhysRevC.87.024320 PACS number(s): 24.75.+i, 25.85.Ca, 21.60.Jz, 27.90.+b

I. INTRODUCTION

The SH nuclei represent the limit of nuclear mass and charge; they inhabit the remote corner of the nuclear landscape whose extent is presently unknown. The mere existence of long-lived SH isotopes has been a fundamental question in science since the late 1950s [1].

Theoretically, it is anticipated that the majority of SH nuclei would fission and/or α decay, but predictions vary from model to model, primarily due to our inability to make accurate predictions for SF half-lives. Here, the main uncertainty is our imperfect knowledge of effective nuclear interactions and the highly nonperturbative effects due to the interplay between the long-ranged electrostatic repulsion and the short-ranged nuclear force. By the end of the 1960s, it had been concluded that the existence of the heaviest nuclei with $Z > 104$ was primarily determined by the quantum-mechanical shell effects (i.e., single-particle motion of protons and neutrons in quantum orbits) [2,3]. These early microscopic-macroscopic (MM) calculations predicted the nucleus with $Z = 114$, $N = 184$ to be the center of an island of long-lived SH nuclei. This result stayed practically unchallenged until the late 1990s when self-consistent mean-field (SMF) models, based on realistic effective interactions, were applied to SH nuclei [4]. Currently, most theories agree that nuclei around $N = 184$ and Z between 114 and 126 should have binding energies strongly lowered by shell effects, which form a region of increased shell stability [5,6].

The use of "hot-fusion" reactions with the neutron-rich ^{48}Ca beam and actinide targets in Dubna resulted in the detection of 48 new nuclides with $Z = 104$–118 and $A = 266$–294 [7]. Several α-decay chains seen in Dubna were independently verified [8]. The most significant outcome of these recent measurements is the observed increase in half-lives with the increasing neutron number—consistent with the predicted increased stability of SH nuclei when approaching $N = 184$. However, the unambiguous identification of the new isotopes still poses a problem because their α-decay chains terminate by SF before reaching the known region of the nuclear chart. The understanding of the competition between α decay and SF channels in SH nuclei is, therefore, of crucial importance for our ability to map the SH region and to assess its extent.

The stability of heavy and SH nuclei is profoundly affected by nuclear deformability through the competing fission valleys that have different geometries. The optimal trajectory in a multidimensional space of collective coordinates that mini-

mizes the collective action can be associated with sequences of intrinsic symmetry-breaking transitions. The effects due to breaking of axial symmetry are known to be important around the first saddle [9–12] and around the second barrier [13,14]. The reflection-asymmetric mode usually contributes at larger elongations, beyond the first barrier [11,12,15,16]. The intrinsic symmetry of the final system—essential for determining the final split—depends on the geometry of the postsaddle and prescission configurations of the nucleus.

The main objective of this paper is to perform realistic predictions of decay modes of SH nuclei by using an SMF approach based on the superfluid nuclear density functional theory (DFT) at the deformed Hartree-Fock-Bogoliubov (HFB) level. The advantage of this method is its ability to properly treat the self-consistent interplay between the electrostatic repulsion and the nuclear attraction [4]. Our calculation—based on a realistic density-dependent effective interaction between nucleons and the microscopic description of the collective action—provides a quantitative description of decay properties of known major and minor actinides. This gives us some confidence in extrapolations to yet-undiscovered regions of SH nuclei. Although several systematic studies of fission barriers of SH nuclei, based on both MM [11,17] and SMF models [13,18–20], have been carried out, fission barriers are not observables that can be directly related to experiment. Moreover, no microscopic survey of SF properties on SH nuclei exists in the literature, except for some MM studies [10,21–24] carried out in constrained deformation spaces and, which lack crucial self-consistent polarization effects, and recent SMF [25,26] calculations limited by symmetry constraints imposed for most nuclei studied. As we point out in this paper, to impose axial and/or space inversion symmetry could result in the overestimation of SF half-lives by many orders of magnitude.

This paper is organized as follows. We review the model used in Sec. II. Section III presents the results of this paper. Finally, the conclusions of our paper are given in Sec. IV.

II. THE MODEL

The phenomenon of fission can be understood in terms of many-body tunneling, which involves mean fields with different intrinsic symmetries [27]. For SH nuclei, the theoretical tool of choice is the self-consistent nuclear DFT [28]. The advantage of DFT is that, while treating the nucleus as a many-body system of fermions, it identifies the essential collective degrees of freedom and provides a starting point for time-dependent extensions [29]. To describe the quantum-mechanical motion under the collective barrier, it is convenient to employ the adiabatic time-dependent HFB (ATDHFB) theory [30,31] that has been successfully applied to fission [32–34].

The Skyrme-HFB calculations were carried out by using the framework previously discussed in Refs. [12,16,34] based on the symmetry-unrestricted DFT solver HFODD [35], capable of breaking all self-consistent symmetries of nuclear mean fields on the way to fission. The nuclear energy density functional was approximated by the SkM* parametrization [36] in the particle-hole channel. The functional SkM* was originally optimized by considering the data on the height of the fission barrier of ^{240}Pu, and this parametrization provides very reasonable results for fission barriers and SF half-lives of even-even actinide nuclei [37–39].

In the particle-particle channel, we employed the density-dependent mixed pairing interaction [40]. To truncate the quasiparticle space of HFB, we adopted the quasi-particle-cutoff value of 60 MeV in the equivalent energy spectrum [41]. As discussed in Ref. [42], such a large value of cutoff energy guarantees the stability of HFB results. The pairing strengths were adjusted to reproduce the neutron and proton pairing gaps in ^{252}Fm [12]; the resulting values are $V_{n0} = -268.9$ MeV fm^3 and $V_{p0} = -332.5$ MeV fm^3. The single-particle basis, which consists of the lowest 1140 stretched states that originate from the 26 major oscillator shells, fully guarantees the stability of HFODD results [43]. All HFB states were taken to compute the mass tensor.

In the constrained SMF approach, the computation of static fission pathways in a multidimensional collective space is fairly straightforward. To this end, one introduces one collective constraint to drive the nucleus from its ground state (g.s.) to scission configurations. In this paper, the mass quadrupole moment Q_{20} was used as a driving constraint that enumerates consecutive points along the one-dimensional static fission path; all remaining multipole moments that represent the multitude of shapes (which include triaxial and reflection-asymmetric shapes) on the way to fission are determined self-consistently. As discussed in our previous papers [12,44], to explore many collective coordinates makes it possible to identify saddle points and valleys [11,45,46] as the competing fission pathways associated with adiabatically varied configurations that are well separated in the collective space when studied in more than one dimension. To eliminate discontinuities in the self-consistent potential-energy surfaces [46] in the vicinity of the saddle points, we locally carried out calculations with two constraints: Q_{20} (elongation) and Q_{22} (triaxiality). Namely, when the quadrupole moment Q_{20} reached the barrier region, we added the axial symmetry-breaking constraint Q_{22}. We then repeated the calculations by releasing the Q_{22} constraint by starting from the previously obtained results. This simplified version of the "additional dimension" method [46] works well, and it allows a reliable estimation of the fission barrier heights. It is only in very few pathological cases of strongly triaxial saddle points (e.g., for the $^{306}_{126}$Uds nucleus) that our method overestimates barrier heights up to 1.7 MeV in comparison with the fully two-dimensional calculation in a (Q_{20}, Q_{22}) plane.

The microscopic ingredients needed to compute the action integral and penetrability are as follows: the collective potential energy, collective inertia (mass tensor), and collective g.s. energy. To calculate the potential energy, from the total HFB energy $E^{\rm tot}(Q_{20})$, we subtract the spurious vibrational zero-point energy ZPE(Q_{20}), obtained by using the Gaussian overlap approximation as in Ref. [47]. In this paper, we use the perturbative HFB cranking expression for the quadrupole mass parameter $B_{20,20}(Q_{20})$ [33,34]. The collective g.s. energy is assumed to be $E_0 = 0.7$ ZPE$(Q_{20}^{\rm g.s.})$. As shown in Fig. 1, the scaling factor of 0.7 improves the agreement between

experiment and theory for the SF half-lives of even-even Fm isotopes without changing the general pattern. Finally, the penetrability has been calculated in the one-dimensional Wentzel-Kramers-Brillouin method according to Ref. [48] by employing action integrals computed along the static fission pathways.

III. RESULTS

To demonstrate that our model is capable of describing experimental observations, Fig. 1 displays predicted SF half-lives for even-even Fm isotopes. This is a challenging case as the measured values [49] vary within this isotopic chain by almost 17 decades. It is satisfying to see quantitative agreement between experiment and theory. Further details of the calculations can be found in Refs. [12,16,33]. Similar calculations performed for the major and minor actinides [38,39] also provide good reproduction of fission barriers and SF half-lives. We wish to stress that good agreement with existing data is a necessary condition for any model to carry out an extrapolation into the unknown region of SH nuclei.

The even-even superheavy nuclei with $108 \leqslant Z \leqslant 126$ and $148 \leqslant N \leqslant 188$ can be divided into three groups according to their g.s. properties [6,50,51]: (i) nuclei with prolate-deformed shapes ($Q_{20} \approx 30$ b) for $N \leqslant 170$, (ii) spherical nuclei for $N > 180$, and (iii) weakly deformed, often triaxial, systems lying between (i) and (iii). The nuclei with $N > 180$ are most stable against SF; they have two-humped barriers with the inner saddle at $Q_{20} \approx 50$ b that is higher than the outer one ($E_A > E_B$). In most cases, triaxiality substantially reduces E_A [13,17,20]. Furthermore, for the reflection-symmetric fission pathways with elongated fragments (sEFs), triaxiality may also reduce E_B [13,14]. Typically, the reflection-asymmetric fission valley that corresponds to asymmetric elongated fragments (aEFs) branches away from the sEF pathway at $Q_{20} > 80$ b beyond the inner saddle. For nuclei with $A > 280$ and $Z > 108$, the outer barrier vanishes along the aEF. SF half-lives of weakly deformed nuclei from the transitional region (iii) were always calculated relative to the prolate-deformed g.s. Both sEF and aEF fission valleys are taken into account in our calculations. The resulting fission probabilities are combined to give the estimated SF half-life; the larger penetrability determines the SF mode.

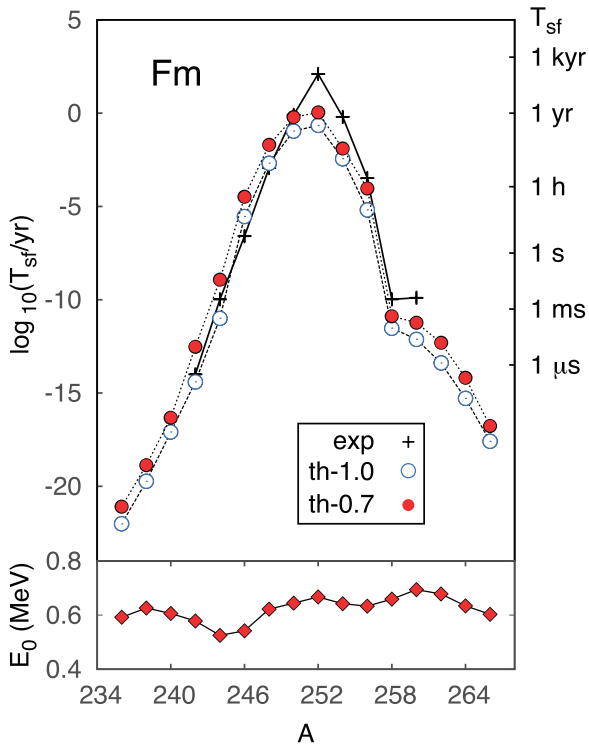

FIG. 1. (Color online) SF half-lives of even-even Fm isotopes with $236 \leqslant A \leqslant 266$, calculated in this paper (th-0.7) compared with experimental data [49]. The corresponding collective ground-state energies $E_0 = 0.7\ \mathrm{ZPE}(Q_{20}^{\mathrm{g.s.}})$ are shown in the lower panel. The scaling factor of 0.7 improves the agreement with experimental data. The results obtained without scaling (th-1.0) are also shown.

To illustrate the competition between sEF and aEF fission pathways, Fig. 2 shows the case of the spherical nucleus $^{306}_{122}$Udd. The energy curves along the reflection symmetric fusion (sFu) and asymmetric fusion (aFu) valleys are also presented. The energy gain due to triaxiality in the region of the first and second saddles can be assessed from the energy curves shown in the inset: The inner barrier is reduced by ∼3 MeV by triaxiality, and the effect around the second saddle is weaker, around 1 MeV. However, the outer barrier vanishes altogether along the aEF, and this favors the reflection-asymmetric fission mode in $^{306}_{122}$Udd. The total density distributions at prescission configurations in aEF and sEF are shown at $Q_{20} \approx 370$ b and $Q_{20} \approx 650$ b, respectively. While the neck rapidly vanishes in aEF, the symmetric prescission region is characterized by an extended neck. Figure 2 also shows the mass parameters $B_{20,20}$ along sEF and aEF pathways. The two $B_{20,20}$ trajectories are fairly similar, which indicates that it is the potential energy

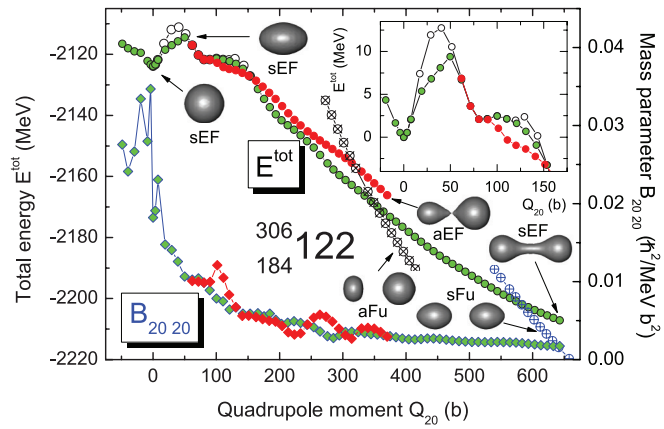

FIG. 2. (Color online) Total energy (circles, left scale) and the quadrupole mass parameter (diamonds, right scale) calculated along the sEF and aEF fission pathways in $^{306}_{122}$Udd together with the corresponding shapes. The energy curves along the symmetric fusion (sFu) and asymmetric fusion (aFu) valleys are also indicated. To illustrate the effect of triaxiality on the inner and outer barriers, the axially symmetric sEF fission pathway is marked by open circles. The deformation energy, normalized with respect to the total g.s. energy, is shown in the inset.

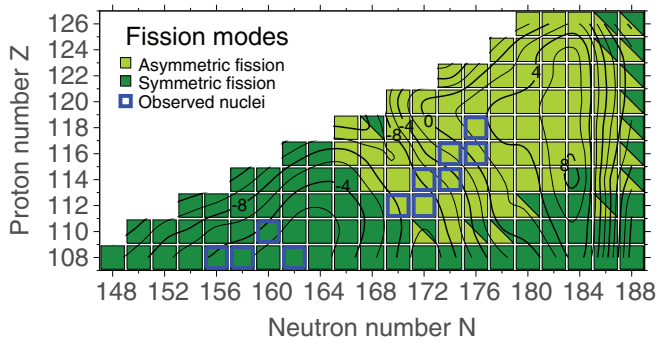

FIG. 3. (Color online) Competition between sEF and aEF SF modes in even-even SH nuclei. The bimodal SF is expected in nuclei with $|\log_{10}(T_{\rm sEF}/T_{\rm aEF})| < 0.3$ marked by coexisting triangles. The experimentally observed nuclei are indicated. The contours show the predicted SF half-lives in logarithmic scale: $\log_{10}(T_{\rm SF}/{\rm s})$.

(in particular, barrier width and height) that determines the optimal fission pathway in this case. The SF half-life along the axially symmetric sEF pathway is $T_{\rm SF} = 10^{13.82}$ s. Triaxial effects along sEF reduce it to $10^{9.39}$ s, and the inclusion of reflection-asymmetric shapes (aEFs) brings the SF half-life of $^{306}_{122}$Udd down to $T_{\rm SF} = 10^{6.25}$ s, which corresponds to an overall reduction in $T_{\rm SF}$ by about 7 orders of magnitude.

The survey of the competition between sEF and aEF SF modes is displayed in Fig. 3. The sEF mode dominates for the Hs isotopes, SH nuclei with $A < 280$, and in a triangle defined by ^{290}Ds, ^{298}Fl, and ^{298}Ds. For the remaining nuclei, the asymmetric mode is expected to win. In very heavy nuclei around $N = 188$, the bimodal fission is predicted. In Fig. 3, the nuclei for which $|\log_{10}(T_{\rm sEF}/T_{\rm aEF})| < 0.3$ are marked by triangles. The barrier heights along aEF and sEF are similar; hence, it is the barrier width that determines the dominant SF mode.

The summary of our survey is given in Fig. 4 and Table I. Figure 4(a) shows the calculated inner fission barrier heights E_A. In the region of SH nuclei with $A < 280$ predicted to have no outer fission barrier, the largest values of E_A (above 7 MeV) are calculated for ^{262,268,270}Hs. In the region of weakly deformed nuclei with $172 \leqslant N \leqslant 180$ that have two-humped barriers (with the inner barrier greater than the outer one), the maximal E_A ($\sim$10 MeV) is calculated for $^{298}_{120}$Udn and $^{300}_{120}$Udn and the minimal barrier (2.7 MeV)—for ^{280,282}Hs. In the region of spherical nuclei with $N > 180$, we expect a sudden drop in E_A from more than 9 MeV for $N = 182, 184$ to less than 5 MeV for $N = 188$. The pattern of fission barriers in SH nuclei obtained in this paper is consistent with that recently predicted by MM models [11,17]. The only difference is that the maximum of E_A is shifted from $Z = 120$ in our paper to $Z = 114$ in both MM models. It is worth noting that the barrier heights of Ref. [11] are close to ours, whereas, those of Ref. [17] are significantly lower (by several MeV). In the recent SMF paper [13], the highest barriers were found for $Z = 120$ with a maximum value of 5.8 MeV for $^{292}_{120}$Udo ($N = 172$).

The calculated SF half-lives are shown in Fig. 4(b). The maximum value of $T_{\rm SF} = 10^{7.75}$ s corresponds to ^{298}Fl, and $T_{\rm SF}$ values of ^{300}Lv and $^{302}_{120}$Udn are similar. The shortest SF half-lives, which reach down to 10^{-10} s, are predicted for nuclei

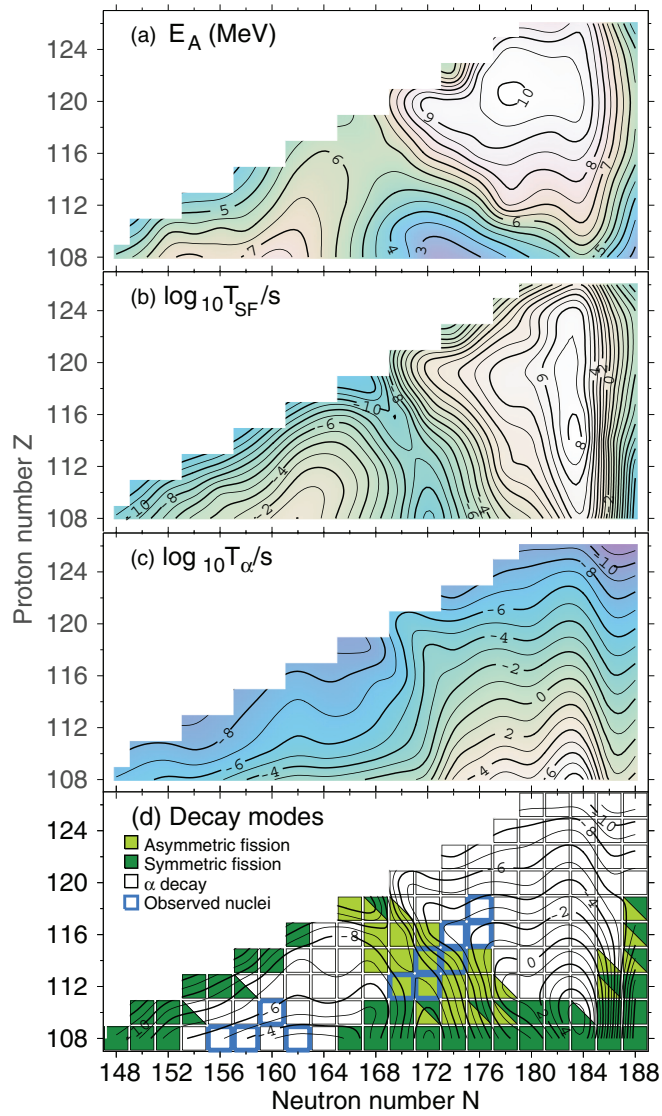

FIG. 4. (Color online) Summary of our SkM* results for even-even SH nuclei. (a) Inner fission barrier heights E_A (in MeV); (b) SF half-lives $\log_{10} T_{\rm SF}$ (in seconds); (c) α-decay half-lives $\log_{10} T_\alpha$ (in seconds); (d) Dominant decay modes. If two modes compete, this is marked by coexisting triangles.

from a narrow corridor formed by ^{280}Hs, ^{284}Fl, and $^{284}_{118}$Uuo that lies on the border of weakly deformed SH nuclei that exhibit prolate-oblate coexistence effects or g.s. triaxiality [6,50,51]. This corridor of fission instability separates the regions of SH nuclei created in hot- and cold-fusion reactions. The imperfect correlation between the pattern of $T_{\rm SF}$ values and the barrier heights displayed in Fig. 4(a) demonstrates that SF half-lives depend on more factors than just E_A. Those include fission barrier width, appearance of the outer barrier, and collective inertia. For instance, our calculation predicts the presence of outer fission barriers around $Z = 114$, and this results in a local increase in $T_{\rm SF}$ in this region.

It is instructive to compare our SF half-lives with other predictions. The MM calculations [23] yield SF half-lives that overshoot our results by more than 5 orders of magnitude.

TABLE I. Summary of SkM* results for the height of the inner fission barrier (E_A), α-decay half-lives ($\log_{10} T_\alpha$), and SF half-lives ($\log_{10} T_{SF}$) of the dominant SF channel: symmetric (S), asymmetric (A), or binary (B).

Z	N	E_A (MeV)	$\log_{10} T_\alpha$ (s)	$\log_{10} T_{SF}$ (s)	Z	N	E_A (MeV)	$\log_{10} T_\alpha$ (s)	$\log_{10} T_{SF}$ (s)	Z	N	E_A (MeV)	$\log_{10} T_\alpha$ (s)	$\log_{10} T_{SF}$ (s)
108	148	5.14	−6.86	−10.68 (S)	**112**	160	5.93	−6.79	−5.46 (S)	**116**	188	5.27	−3.24	−7.39 (B)
	150	5.81	−6.28	−8.74 (S)		162	6.61	−6.20	−2.74 (S)	**118**	166	5.54	−9.12	−12.09 (A)
	152	6.83	−5.79	−6.59 (S)		164	6.32	−6.57	−2.09 (S)		168	5.84	−8.80	−12.00 (B)
	154	7.10	−5.83	−4.73 (S)		166	5.91	−6.45	−3.05 (S)		170	7.01	−6.22	−6.07 (A)
	156	6.78	−5.13	−3.64 (S)		168	5.14	−5.87	−5.06 (S)		172	8.32	−3.78	−1.20 (A)
	158	7.10	−4.03	−2.45 (S)		170	4.53	−4.72	−8.03 (A)		174	9.11	−4.01	0.93 (A)
	160	7.71	−3.08	−0.91 (S)		172	4.32	−2.99	−9.15 (A)		176	9.19	−3.18	2.91 (A)
	162	7.35	−2.52	0.01 (S)		174	4.75	−0.15	−6.65 (A)		178	9.47	−2.98	4.65 (A)
	164	6.40	−2.63	−1.18 (S)		176	5.56	1.09	−2.93 (A)		180	9.27	−3.35	4.76 (A)
	166	5.52	−2.31	−3.16 (S)		178	7.45	1.72	1.53 (A)		182	9.14	−2.36	7.00 (A)
	168	4.51	−1.73	−5.56 (S)		180	7.12	1.45	2.16 (B)		184	9.30	−2.61	6.18 (A)
	170	3.87	−1.17	−8.14 (S)		182	7.06	3.29	5.26 (S)		186	7.44	−5.12	−0.69 (A)
	172	2.70	−0.41	−11.22 (S)		184	7.41	3.20	6.34 (S)		188	5.51	−4.81	−6.50 (B)
	174	2.65	3.13	−8.74 (S)		186	5.82	−0.95	−2.20 (B)	**120**	170	7.83	−5.51	−3.86 (A)
	176	2.98	4.44	−5.40 (S)		188	3.81	−0.58	−11.56 (S)		172	9.23	−5.55	0.14 (A)
	178	3.49	5.64	−2.33 (S)	**114**	158	4.45	−8.27	−11.16 (S)		174	9.15	−5.75	1.23 (A)
	180	4.04	5.14	−0.95 (S)		160	5.32	−7.51	−8.46 (S)		176	9.48	−5.10	2.89 (A)
	182	4.42	7.34	1.69 (S)		162	6.19	−6.93	−5.53 (S)		178	10.05	−4.98	4.28 (A)
	184	5.36	7.99	4.58 (S)		164	6.19	−7.37	−4.20 (S)		180	9.91	−5.14	5.09 (A)
	186	3.87	1.86	−3.11 (S)		166	5.98	−7.36	−4.65 (S)		182	9.82	−4.06	7.13 (A)
	188	2.80	2.53	−12.85 (S)		168	5.52	−6.51	−7.12 (A)		184	9.54	−4.23	6.38 (A)
110	150	4.59	−7.53	−11.35 (S)		170	5.32	−5.51	−9.34 (A)		186	7.62	−6.51	0.15 (A)
	152	5.89	−7.40	−8.76 (S)		172	5.69	−3.45	−7.53 (A)		188	5.64	−6.25	−5.63 (B)
	154	5.85	−7.79	−7.50 (S)		174	6.24	−1.49	−5.06 (A)	**122**	174	6.23	−8.00	−4.42 (A)
	156	6.16	−7.38	−5.25 (S)		176	7.13	−0.31	−1.43 (A)		176	9.22	−7.12	−0.54 (A)
	158	6.02	−6.59	−4.76 (S)		178	8.14	0.17	1.96 (A)		178	9.90	−6.62	2.11 (A)
	160	6.74	−5.77	−3.10 (S)		180	7.82	−0.08	2.87 (A)		180	9.86	−6.46	3.12 (A)
	162	7.01	−5.17	−1.04 (S)		182	7.82	1.37	6.30 (A)		182	9.65	−5.51	6.15 (A)
	164	6.43	−5.42	−1.03 (S)		184	7.97	1.22	7.75 (S)		184	9.38	−5.73	6.25 (A)
	166	5.63	−5.16	−2.41 (S)		186	6.34	−2.39	−2.49 (A)		186	7.42	−7.87	0.01 (A)
	168	4.59	−4.53	−4.79 (S)		188	4.57	−1.84	−9.20 (B)		188	5.42	−7.65	−5.40 (B)
	170	3.63	−3.64	−7.53 (S)	**116**	162	5.69	−7.81	−9.43 (S)	**124**	178	9.51	−7.96	−0.66 (A)
	172	3.18	−2.23	−10.27 (B)		164	6.04	−8.18	−7.48 (S)		180	9.43	−7.68	2.75 (A)
	174	3.41	1.39	−7.65 (A)		166	5.85	−7.95	−7.31 (A)		182	9.33	−7.08	5.49 (A)
	176	4.12	2.67	−3.86 (B)		168	5.89	−7.25	−9.16 (A)		184	9.12	−7.30	5.67 (A)
	178	4.88	3.61	−0.43 (B)		170	6.01	−6.54	−9.59 (A)		186	7.08	−9.44	−1.37 (B)
	180	5.21	3.19	0.80 (S)		172	7.16	−3.64	−4.24 (A)		188	5.03	−9.26	−6.00 (B)
	182	5.84	5.25	3.79 (S)		174	7.84	−2.69	−1.88 (A)	**126**	180	8.20	−9.26	−2.11 (A)
	184	6.73	5.45	5.42 (S)		176	8.72	−1.67	0.96 (A)		182	8.05	−9.27	0.48 (A)
	186	5.24	0.36	−2.38 (S)		178	8.84	−1.36	3.45 (A)		184	8.70	−9.47	1.83 (A)
	188	3.27	0.87	−12.36 (S)		180	8.54	−1.66	3.91 (A)		186	6.27	−11.54	−4.58 (B)
112	154	4.66	−8.89	−10.81 (S)		182	8.53	−0.48	6.70 (A)		188	4.12	−11.36	−8.84 (B)
	156	4.75	−8.33	−9.50 (S)		184	8.58	−0.77	7.27 (A)					
	158	5.20	−7.57	−7.72 (S)		186	7.07	−3.78	−1.26 (A)					

We attribute this to the assumption of axiality and reflection-symmetry used in their paper. Likewise, the axially symmetric HFB + D1S calculation [26] overestimates our SF half-lives by many orders of magnitude. On the other hand, there is a nice consistency between our aEF results and those obtained in the axial Skyrme HF + BCS approach of Refs. [25] with SV-min and SV-bas functionals. In particular, the corridor of the maximum SF instability is predicted similarly by both approaches. It is anticipated, however, that the inclusion of triaxiality is likely to reduce their SF half-lives significantly.

Figure 4(c) summarizes our $\log_{10} T_\alpha$ values. To estimate α-decay half-lives, we used the standard Viola-Seaborg expression [52] with the parameters from Ref. [53] and calculated Q_α values of Fig. 5. In general, we obtain a reasonable agreement with experiment. Our model underestimates the experimental Q_α values in the vicinity of the deformed shell

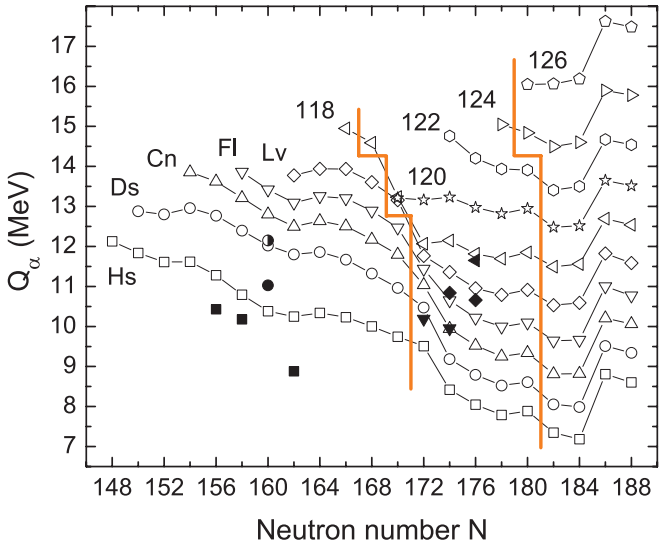

FIG. 5. (Color online) Calculated (open symbols) and observed (full symbols) Q_α values for SH nuclei. The experimental data, attributed to a high-K isomeric state in ^{270}Ds [54], are marked by a half-circle. The borders between three regions of SH nuclei, prolate deformed for $N \leqslant 170$, γ soft for $172 \leqslant N \geqslant 180$, and spherical for $N > 180$, are marked by thick lines.

closure $N = 162$. In this respect, the predictions of Refs. [23,26] are closer to the data.

Our survey of lifetimes of even-even SH nuclei is summarized in Fig. 4(d). According to our model, the region of long-lived SH nuclei is expected to be centered on ^{294}Ds with a predicted total half-life (considering SF and α decay) of $10^{5.13}$ s, i.e., ∼1.5 days. For comparison, the total half-life for ^{292}Ds predicted in Refs. [23,26] is 51 and 14 yr, respectively.

IV. CONCLUSIONS

To summarize, we carried out self-consistent Skyrme-HFB calculations to predict main decay modes of even-even SH nuclei with $108 \leqslant Z \leqslant 126$ and $148 \leqslant N \leqslant 188$, to assess their lifetimes, and to estimate the center of enhanced stability in the SH region. In our model, fission pathways in the collective space are not constrained by imposed self-consistent symmetries, and ATDHFB cranking fission inertia and zero-point energy corrections have been obtained microscopically. The model satisfactorily reproduces experimental T_{SF} values in even-even actinides, which is a necessary condition for a model-based extrapolation for unknown SH nuclei. We wish to emphasize that our survey is a systematic self-consistent approach to SF in SH nuclei, which is free from artificially imposed symmetry constraints that are likely to affect previous predictions.

We predict two competing SF modes in SH nuclei: the reflection-symmetric mode sEF and the reflection-asymmetric mode aEF. The latter one is expected to prevail for $N \geqslant 166$, whereas, sEF shows up in the region of light SH nuclei and for neutron-rich nuclei with $N \approx 188$. The region of asymmetric fission roughly corresponds to the region of the highest SF barriers and longest SF half-lives.

The predicted SF half-lives of even-even transitional nuclei around ^{284}Cn are dramatically reduced as compared to the current experimental estimates [7]. Since those systems belong to the region of shape coexistence and/or oblate g.s. shapes, some further increase in SF half-lives is anticipated due to the lowering of g.s. energy due to the shape mixing and/or appearance of a triaxial saddle at low deformations [6,20,24,51]. Other improvements of the current model include dynamical treatment of penetrability by considering several collective coordinates, improved energy density functionals [37], and the full ATDHFB inertia [34]. Work along these lines is in progress.

ACKNOWLEDGMENTS

Discussions with J. Dobaczewski are gratefully acknowledged. This work was supported by the National Nuclear Security Administration under the Stewardship Science Academic Alliances program through DOE Grant No. DE-FG52-09NA29461, by the US Department of Energy under Contract No. DE-FG02-96ER40963 (University of Tennessee), by the NEUP Grant No. DE-AC07-05ID14517 (sub-Grant No. 00091100), and by the National Science Center (Poland) under Contract No. DEC-2011/01/B/ST2/03667.

[1] G. Scharff-Goldhaber, Nucleonics **15**, 122 (1957).
[2] W. D. Myers and W. J. Swiatecki, Nucl. Phys. **81**, 1 (1966).
[3] A. Sobiczewski, F. A. Gareev, and B. N. Kalinkin, Phys. Lett. **22**, 500 (1966); S. Nilsson *et al.*, Nucl. Phys. A **131**, 1 (1969).
[4] S. Ćwiok, J. Dobaczewski, P.-H. Heenen, P. Magierski, and W. Nazarewicz, Nucl. Phys. A **611**, 211 (1996).
[5] A. T. Kruppa, M. Bender, W. Nazarewicz, P.-G. Reinhard, T. Vertse, and S. Ćwiok, Phys. Rev. C **61**, 034313 (2000); M. Bender, W. Nazarewicz, and P.-G. Reinhard, Phys. Lett. B **515**, 42 (2001).
[6] S. Ćwiok, P.-H. Heenen, and W. Nazarewicz, Nature (London) **433**, 705 (2005).
[7] Y. T. Oganessian *et al.*, Phys. Rev. Lett. **104**, 142502 (2010); **108**, 022502 (2012); **109**, 162501 (2012); Y. T. Oganessian, J. Phys. G **34**, R165 (2007); Acta Phys. Pol. B **43**, 167 (2012).
[8] L. Stavsetra, K. E. Gregorich, J. Dvorak, P. A. Ellison, I. Dragojevic, M. A. Garcia, and H. Nitsche, Phys. Rev. Lett. **103**, 132502 (2009); C. E. Düllmann *et al.*, *ibid.* **104**, 252701 (2010).
[9] S. E. Larsson, I. Ragnarsson, and S. G. Nilsson, Phys. Lett. B **38**, 269 (1972); M. Girod and B. Grammaticos, Phys. Rev. C **27**, 2317 (1983).
[10] A. Baran, K. Pomorski, A. Łukasiak, and A. Sobiczewski, Nucl. Phys. A **361**, 83 (1981).
[11] P. Möller, A. J. Sierk, T. Ichikawa, A. Iwamoto, R. Bengtsson, H. Uhrenholt, and S. Åberg, Phys. Rev. C **79**, 064304 (2009).
[12] A. Staszczak, A. Baran, J. Dobaczewski, and W. Nazarewicz, Phys. Rev. C **80**, 014309 (2009).
[13] H. Abusara, A. V. Afanasjev, and P. Ring, Phys. Rev. C **85**, 024314 (2012).

[14] B.-N. Lu, E.-G. Zhao, and S.-G. Zhou, Phys. Rev. C **85**, 011301(R) (2012).
[15] J. R. Nix, Nucl. Phys. A **130**, 241 (1969).
[16] A. Staszczak, A. Baran, and W. Nazarewicz, Int. J. Mod. Phys. E **20**, 552 (2011).
[17] M. Kowal, P. Jachimowicz, and A. Sobiczewski, Phys. Rev. C **82**, 014303 (2010).
[18] T. Bürvenich, M. Bender, J. A. Maruhn, and P.-G. Reinhard, Phys. Rev. C **69**, 014307 (2004).
[19] S. Karatzikos, A. Afanasjev, G. Lalazissis, and P. Ring, Phys. Lett. B **689**, 72 (2010).
[20] V. Prassa, T. Nikšić, G. A. Lalazissis, and D. Vretenar, Phys. Rev. C **86**, 024317 (2012).
[21] P. Möller, J. Nix, and W. Swiatecki, Nucl. Phys. A **492**, 349 (1989).
[22] A. Staszczak, Z. Łojewski, A. Baran, B. Nerlo-Pomorska, and K. Pomorski, in *Proceedings of the 3rd International Conference: Dynamical Aspects of Nuclear Fission, Častá-Papiernička, 1996*, edited by J. Kliman and B. I. Pustylnik (JINR, Dubna, 1996), p. 22.
[23] R. Smolańczuk, J. Skalski, and A. Sobiczewski, Phys. Rev. C **52**, 1871 (1995); R. Smolańczuk, *ibid.* **56**, 812 (1997).
[24] R. Gherghescu, J. Skalski, Z. Patyk, and A. Sobiczewski, Nucl. Phys. A **651**, 237 (1999).
[25] J. Erler, K. Langanke, H. P. Loens, G. Martinez-Pinedo, and P.-G. Reinhard, Phys. Rev. C **85**, 025802 (2012); N. Schindzielorz, J. Erler, P. Klüpfel, and P.-G. Reinhard, Int. J. Mod. Phys. E **18**, 773 (2009).
[26] M. Warda and J. L. Egido, Phys. Rev. C **86**, 014322 (2012).
[27] H. J. Krappe and K. Pomorski, *Theory of Nuclear Fission: A Textbook*, Lecture Notes in Physics Vol. 838 (Springer, Berlin, 2012).
[28] M. Bender, P.-H. Heenen, and P.-G. Reinhard, Rev. Mod. Phys. **75**, 121 (2003).
[29] H. Goutte, J. F. Berger, P. Casoli, and D. Gogny, Phys. Rev. C **71**, 024316 (2005).
[30] M. Baranger and M. Véneroni, Ann. Phys. **114**, 123 (1978); J. Dobaczewski and J. Skalski, Nucl. Phys. A **369**, 123 (1981); F. Grümmer, K. Goeke, and P.-G. Reinhard, *Quantized ATDHF: Theory and Realistic Applications to Heavy Ion Fusion*, Lecture Notes in Physics Vol. 171 (Springer, Berlin, 1982), p. 323.
[31] J. Skalski, Phys. Rev. C **77**, 064610 (2008).
[32] E. Yuldashbaeva, J. Libert, P. Quentin, and M. Girod, Phys. Lett. B **461**, 1 (1999).
[33] A. Baran, A. Staszczak, and W. Nazarewicz, Int. J. Mod. Phys. E **20**, 557 (2011).
[34] A. Baran, J. A. Sheikh, J. Dobaczewski, W. Nazarewicz, and A. Staszczak, Phys. Rev. C **84**, 054321 (2011).
[35] N. Schunck, J. Dobaczewski, J. McDonnell, W. Satuła, J. A. Sheikh, A. Staszczak, M. Stoitsov, and P. Toivanen, Comput. Phys. Commun. **183**, 166 (2012).
[36] J. Bartel, P. Quentin, M. Brack, C. Guet, and H. B. Håkansson, Nucl. Phys. A **386**, 79 (1982).
[37] M. Kortelainen, J. McDonnell, W. Nazarewicz, P.-G. Reinhard, J. Sarich, N. Schunck, M. V. Stoitsov, and S. M. Wild, Phys. Rev. C **85**, 024304 (2012).
[38] J. McDonnell, Ph.D. thesis, The University of Tennessee, Knoxville, USA, 2012.
[39] J. McDonnell, N. Schunck, and W. Nazarewicz, arXiv:1301.7587.
[40] J. Dobaczewski, W. Nazarewicz, and M. Stoitsov, Eur. Phys. J. A **15**, 21 (2002).
[41] J. Dobaczewski, H. Flocard, and J. Treiner, Nucl. Phys. A **422**, 103 (1984); J. Dobaczewski, W. Nazarewicz, T. R. Werner, J.-F. Berger, C. R. Chinn, and J. Dechargé, Phys. Rev. C **53**, 2809 (1996).
[42] P. J. Borycki, J. Dobaczewski, W. Nazarewicz, and M. V. Stoitsov, Phys. Rev. C **73**, 044319 (2006); J. C. Pei, A. T. Kruppa, and W. Nazarewicz, *ibid.* **84**, 024311 (2011).
[43] A. Staszczak, J. Dobaczewski, and W. Nazarewicz, Int. J. Mod. Phys. E **14**, 395 (2005).
[44] M. Warda, A. Staszczak, and W. Nazarewicz, Phys. Rev. C **86**, 024601 (2012).
[45] P. Möller, D. G. Madland, A. J. Sierk, and A. Iwamoto, Nature (London) **409**, 785 (2001).
[46] N. Dubray and D. Regnier, Comput. Phys. Commun. **183**, 2035 (2012).
[47] A. Staszczak, S. Piłat, and K. Pomorski, Nucl. Phys. A **504**, 589 (1989); A. Baran, A. Staszczak, J. Dobaczewski, and W. Nazarewicz, Int. J. Mod. Phys. E **16**, 443 (2007).
[48] J. N. Leboeuf and R. C. Sharma, Can. J. Phys. **51**, 446 (1973); **51**, 1148 (1973); **51**, 2023 (1973).
[49] N. Holden and D. Hoffman, Pure Appl. Chem. **72**, 1525 (2000); J. Khuyagbaatar *et al.*, Eur. Phys. J. A **37**, 177 (2008).
[50] P. Jachimowicz, M. Kowal, and J. Skalski, Phys. Rev. C **83**, 054302 (2011).
[51] P. Möller, A. Sierk, R. Bentsson, H. Sagawa, and T. Ichikawa, At. Data Nucl. Data Tables **98**, 149 (2012).
[52] V. E. Viola, Jr. and G. T. Seaborg, J. Inorg. Nucl. Chem. **28**, 741 (1966).
[53] A. Parkhomenko and A. Sobiczewski, Acta Phys. Pol. B **36**, 3095 (2005).
[54] S. Hofmann *et al.*, Eur. Phys. J. A **10**, 5 (2001).